HHS Public Access

Author manuscript

Oncogene. Author manuscript; available in PMC 2017 May 05.

Published in final edited form as:

Oncogene. 2017 February 02; 36(5): 639–651. doi:10.1038/onc.2016.229.

Exosomes miR-126a released from MDSC induced by DOX treatment promotes lung metastasis

Zhongbin Deng[2,*], **Yuan Rong**[2], **Yun Teng**[2], **Xiaoying Zhuang**[2], **Abhilash Samykutty**[2], **Jingyao Mu**[2], **Lifeng Zhang**[2], **Pengxiao Cao**[2], **Jun Yan**[2], **Donald Miller**[2], and **Huang-Ge Zhang**[1,2,*]

[1]Robley Rex VA Medical Center, Louisville, KY 40206

[2]James Graham Brown Cancer Center, Department of Microbiology & Immunology, University of Louisville, KY 40202

Abstract

Acquired resistance to chemotherapy remains a major stumbling block in cancer treatment. Chronic inflammation plays a crucial role in induction of chemo resistance, and results in part from the induction and expansion of inflammatory cells that include myeloid derived suppressor cells (MDSC) and IL-13^{+}Th2 cells. The mechanisms that lead to induction of activated MDSCs and IL-13^{+}Th2 cells have not yet been identified. Here we demonstrated that doxorubicin treatment of 4T1 breast tumor bearing mice led to the induction of IL-13R^{+}miR-126a^{+}MDSC (DOX-MDSC). DOX-MDSC promote breast tumor lung metastasis through MDSC miR-126a^{+}exosomal mediated induction of IL-13^{+}Th2 cells and tumor angiogenesis. The induction of DOX-MDSC is regulated in a paracrine manner. DOX treatment not only increases IL-33 released from breast tumor cells, which is crucial for the induction of IL-13^{+}Th2 cells, but it also participates in the induction of IL-13 receptors and miR-126a expressed on/in the MDSCs. IL-13 released from IL-13^{+}Th2 cells then promotes the production of DOX-MDSC and MDSC miR-126a^{+}exosomes via MDSC IL-13R. MDSC miR-126a^{+}exosomes further induce IL13^{+}Th2 cells in a positive feed-back loop manner. We also showed that MDSC miR-126a rescues doxorubicin induced MDSC death in a S100A8/A9 dependent manner and promotes tumor angiogenesis. Our findings provide insight into the MDSC exosomal mediated chemo resistance mechanism, which will be useful for the design of inhibitors targeting the blocking of induction of miR-126a^{+}MDSC.

Keywords

MDSC; exosomal miR-126a; chemo resistance; breast metastasis; IL13Th2 T cells

[*]Address correspondence and reprint requests to: Dr. Huang-Ge Zhang, James Brown Cancer Center, University of Louisville, CTRB 309, 505 Hancock Street, Louisville, KY 40202, H0Zhan17@louisville.edu or z0deng01@louisville.edu.

The authors declare that they have no competing financial interests

Author Contributions: All authors designed the experiments, analyzed and interpreted the results and wrote the paper. Z-B, D., J.M., and X.Z. performed the experiments.

Introduction

Although chemo/radiation therapy (CRT) is one of the most common treatments for cancer patients, chemotherapy fails to kill all cancer cells because of intrinsic or acquired drug resistance. Acquired resistance accounts for >90% of unsuccessful treatments in advanced cancer patients. CRT induces inflammation by activation of a number of inflammatory cells including myeloid derived suppressor cells (MDSC)[43], IL-13^{+}Th2 cells[4220] and endothelial cells[34]. Inflammation activates a number of pathways that contribute to the chemo resistance[47]. Therefore, there is a dire need for understanding the inflammation associated cellular and molecular pathways leading to chemo resistance and further development of novel strategies to block/reverse chemo resistance would also yield a new and practical therapeutic method for treatment of cancer patients.

MDSCs are a heterogenic and immunosuppressive subset of cells that promote tumor vasculogenesis and tumor progression. Recent findings reported that chemotherapy induces MDSC resulting in attenuation of the anticancer efficacy of the chemotherapy[6, 16]. Chemotherapy also causes an increase in MDSC numbers in breast cancer patients[13, 33] and melanoma[29, 45] and enhances immunosuppression. Blocking MDSC actions reverses docetaxel chemo resistance in a mouse model of prostate cancer[54]. How MDSCs mediate development of chemo resistance is not well studied.

Exosomes mediated drug resistance has been identified across a broad spectrum of tumors[4, 5, 9, 21, 48]. Despite a growing number of studies demonstrating MDSC released exosomes play a role in immune suppression[7], it is unknown whether the exosomes released from chemotherapeutic drug treated versus non-treated MDSCs have different biological activities in terms of regulating tumor progression and chemo resistance. More specifically understanding whether MDSC exosomes facilitate development of chemotherapy resistance via remodeling host immune responses is needed for further elucidating the role of chemo drug induced MDSC exosomes in disease progression, metastasis, and response to treatment.

One of the mechanisms underlying tumor exosomes mediated drug resistance and tumor immune escape is likely to the exporting of harmful factors from tumor cells to immune cells. Exosomes are enriched with non-coding RNA, including miRNA. MicroRNAs (miRNAs) are a class of small, non-coding RNAs that post-transcriptionally control the translation and stability of mRNAs. Hundreds of miRNAs are known to have dysregulated expression in cancer[24, 25, 40]. miRNAs could act as tumor suppressors or oncogenes depending on the interactions of mRNA and various factors. In this study, we investigated the role of MDSC exosomal miR-126a on lung metastasis of the murine breast tumor since exosomal miR-126a released from MDSCs is enriched upon doxorubicin treatment. miR-126a has been shown to be both a tumor suppressor and an oncogene depending on the type of cancer studied[28]. Overexpression of miR-126a in tumor cells inhibits tumor growth through the inhibition of expression of genes related to tumor cell cycles[14]. miR-126a also supports cancer progression[12,41] through the promotion of blood vessel formation[17, 38,2] and inflammation[53] at the site of activation of other types of cancer. High miR-126 expression in acute myeloid leukemia was associated with poor survival and higher chance of relapse[12].

The cellular and molecular mechanisms underlying these discrepancies in terms of response to miR-126a are not known. The role of chemotherapy induced miR-126a in MDSCs in terms of tumor progression, and subsequent biological effect of miR-126a delivered by MDSC exosomes on the recipient cells has not been studied, although it was reported that miR-126 controls the survival and function of plasmacytoid dendritic cells[2].

It is known that Th2 polarization of tumor microenvironments via type 2 cytokines promotes tumor metastasis and contributes to chemo resistance. Inflammation induced miR-126 accelerates the development of allergic airways disease through induction of Th2 T cells[27]. Recent studies show that induction of the production of IL-33 by chemotherapeutic agents is crucial for the induction of type 2 immune responses by promoting the synthesis of cytokines such as IL-13[18, 32]. IL-33-driven Th2 cells are rapid and potent producers of the type 2 cytokine IL-13[15, 37] and may contribute to carcinogenesis. Exosomes have been known to play a crucial role in intercellular communication. Whether MDSC derived exosomes play a role in induction of chemo resistance through cross-talking with IL-13^{+}Th2 T cells is not known. Furthermore, whether exosome mediated MDSC-IL-13^{+}Th2 cell interactions contribute to chemo resistance is an entirely novel topic.

Although tumor-derived exosomes are emerging as mediators of tumorigenesis, the role of MDSC-derived exosomes has not been fully understood. In this study, using the murine breast cancer model as a proof of concept, we tested the hypothesis that exporting miR-126a via MDSC exosomes is one of the important mechanisms underlying chemo resistance. We explored the function of MDSC-derived exosomes in metastasis in mice. MDSC exosomes from highly metastatic breast tumor increased the metastatic behavior of primary tumors by permanently cross-talking with Th2 T cells and endothelial cells through MDSC exosomal miR-126a. Anti-miR-126a therapy decreased DOX treatment induced resistance and reduced tumor growth and metastasis. In addition, we identified that MDSC-derived exosomes also prevent DOX induced MDSC death by upregulating expression of S100A8/A9. Our data show that MDSC exosomes induced by DOX treatment supports metastasis, has prognostic value and offers promise for new therapeutic directions in the metastatic process.

Results

Doxorubicin treatment induces MDSC through an IL-33/IL-13 mediated pathway in metastatic lung lesions

Given that proinflammatory cytokines have been associated with the severity of chemotherapy-induced mucositis[18], we hypothesize that pulmonary toxicity caused by doxorubicin (DOX) may result in an immune-mediated hypersensitivity reaction. To test this hypothesis, 4T1 breast tumor bearing mice were treated with DOX (5mg/kg) at 15 days post-tumor implantation. We observed the production of IL-33 and that its soluble receptor sST2 was significantly elevated in lung tissue extracts from 4T1 tumor-bearing mice systemically treated with DOX as compared with that of the vehicle-treated control (VEH) mice (Fig. 1A). Immunohistochemistry staining confirmed that IL-33 was most prominently detected in DOX-treated lung epithelial cells in lung (Fig. 1B). IL-33/ST2 is crucial for the induction of type 2 immune responses by promoting the synthesis of cytokines such as IL-13 by Th2 lymphocytes[35, 39]. After DOX treatment, we found that infiltration of lung by

IL-4$^+$IL-13$^+$CD4$^+$Th2 cells was increased significantly (Fig. 1C–D) in addition to Th1 and Th17 T cell increases reported by others[6] (Supplementary Fig. **1A**). The results were also repeated in the C57BL/6-mouse-derived E0771 model of spontaneously metastatic mammary cancer and CT-26 colon cancer model (Supplementary Fig. **2A–F**). GATA3 is one of the crucial molecules that induce Th2 cells while suppressing their differentiation towards Th1 cells. CD4$^+$ T lymphocytes isolated from DOX-treated mice exhibited elevated expression of GATA-3 mRNA and the percentages of GATA3$^+$ CD4$^+$T cells and STAT6$^+$ CD4$^+$T cells (Supplementary Fig. **1B–C**), when compared with vehicle-treated mice. Collectively, those data indicate that Th2 effector lineage was expanded in the lung of tumor bearing mice response to DOX treatment.

We also found that DOX treatment increased the levels of chemokines including CXCL1/2 and CCL2 in mice (Supplementary Fig. **1D**) compared to mice treated with PBS as a control. CXCL1/2 and CCL2 have a role in recruitment of immature myeloid cells (CD11b$^+$Gr-1$^+$) to sites of inflammation. In agreement with data published by others[3], a reduction in the proportion and the number of MDSCs in the spleen of DOX-treated tumor-bearing mice was observed. However, in contrast to MDSCs in the spleen, the proportion of MDSCs was significantly increased in the lungs of treated mice when compared to the untreated mice (Fig. 1E). The data generated from Real time-PCR analysis further indicate that DOX increased the expression of the immunosuppression genes encoding for arginase 1 (Arg1) and TGF-β and decreased genes encoding for inducible nitric oxide synthase 2 (Nos2) and TNF-α in the lung of MDSC tumor-bearing mice when compared with mice treated with PBS (Supplementary Fig. **3A**). Most notable was the detection of S100A8/9, known to play a role in promoting tumor lung metastasis[1], which was expressed in abundance in DOX-induced CD11b$^+$Gr1$^+$ cells (Supplementary Fig. **3A**). Induction of DOX-treated MDSCs is associated with increased expression of IL-13alpha1R (Supplementary Fig. **3A**). Therefore, DOX treatment might lead to induction of Arg1 and S100A9 in MDSCs via IL-13. To address this, we assessed the ability of IL-13 to induce expression of Arg1 and S100A9 in MDSCs in vivo and in vitro. IL-13 alone significantly induced Arg1 expression in MDSCs compared with vehicle-treated MDSCs (Fig. 1F); whereas the expression of NOS2 was suppressed. Interestingly, IL-13-induced Arg1 and S100A9 expression was enhanced significantly by the presence of IL-33 which expands functional MDSCs. However, DOX in combination with IL-13, with IL-33 or both IL-13 and IL-33 had no additional effect on the induction of Arg1 and S100A9 expression compared to IL-13, IL-13 or both IL-13 and IL-33 (Fig. 1F). To determine whether IL-13 produced by CD4$^+$ T cells is involved in inhibition of the M1 cytokine profile, mainly IL-12 and TNF-α, primary MDSC or IFN-γ/LPS stimulated MDSCs were co-cultured with lung CD4 cells isolated from vehicle and DOX-treated tumor bearing mice. We found that addition of DOX-treated CD4$^+$ T cells reduced the secretion of TNF-α and IL-12 more than addition of vehicle-treated CD4$^+$ T cells (Fig. 1G). This effect was reversed in the presence of anti-IL-13 antibody (Fig. 1G), indicating that CD4$^+$ T lymphocytes isolated from DOX-treated tumor bearing mice inhibit the production of IL-12 and TNF-α via an IL-13 mediated signaling pathway.

DOX-induced MDSCs promote tumor growth, angiogenesis and metastasis with T cells participation

To study the biological effects of DOX-induced $CD11b^+Gr1^+$ cells on tumor progression, lung $CD11b^+Gr1^+$ cells from 4T1-derived tumors of vehicle- or DOX-treated mice were sorted by FACS and then co-injected with 4T1 cells. Tumor bearing mice were continuously treated by intra-tumor injection of FACS sorted $CD11b^+Gr1^+$ cells on day 5 and 10 post-tumor challenge. We found that DOX-MDSC treated mice had faster growth tumor than vehicle (VEH-MDSC) treated mice (Fig. 2A). DOX-MDSCs not only promoted tumor growth, but co-injection of DOX-MDSCs also promotes tumor metastasis to the lung (Fig. 2B). Both immunosuppression and angiogenesis mediated by MDSCs played a role in tumor growth and metastasis[11, 26, 36]. Still unknown was whether DOX-MDSCs promote new blood vessel formation. The effect of DOX-MDSCs on tumor blood vessel development was evaluated by immunostaining tumor tissue. The data generated from CD31 (a marker of endothelia cells) stained tumor tissue indicates that DOX-MDSCs increases the numbers of $CD31^+$ blood vessels (Fig. 2C). This conclusion was further confirmed by an in vitro blood vessel tube formation assay. Compared with VEH-MDSCs, DOX-MDSCs had a substantially higher proangiogenic capacity as indicated by an increased tube formation capacity in the EC-co-culture assay (Fig. 2D). To assess whether DOX-MDSCs could affect angiogenesis by producing soluble proangiogenic factors, we sorted lung DOX-MDSCs and VEH-MDSCs from 4T1 tumor-bearing mice and cultured the cells in vitro for 5 days. Then, we analyzed the presence of soluble pro-/antiangiogenic factors in their supernatants with the Mouse Angiogenesis Array Kit. DOX-MDSC culture supernatants had higher amounts of matrix metalloproteinase (MMP)-9, osteopontin (OPN), SDF-1, and CXCL1 detected when compared to VEH-MDSC cultures (Fig. 2E). The induction of MMP-9, OPN, SDF-1, and CXCL1 is specific since the levels of other proteins as listed in the figure 2E were not altered. The results from real-time PCR further confirmed that the expression of MMP-9, SDF-1 and CXCL1 were higher than in the VEH-MDSC (Supplementary Fig. **3B**). We further confirmed the array based CXXL1 result with a standard ELISA (Supplementary Fig. **3C**).

Since $IL\text{-}4^+IL\text{-}13^+CD4^+$Th2 cells were increased significantly, we decided to determine whether T cells play a role in the MDSC-mediated tumor progression using $Rag1^{-/-}$ mice. In contrast to DOX-MDSC isolated from wild-type 4T1 tumor bearing mice, DOX-MDSC from $Rag1^{-/-}$ mice, which lack T cells, have lost the capacity to promote tumor progression (Fig. 2A–B).

Exosomes released from DOX-MDSC enhance Th2 cell responses and tumor angiogenesis in the lung of tumor bearing mice

Given the fact that DOX-MDSCs have a role in promoting tumor progression via an interaction with $CD4^+$ T cells and endothelia cells, and because cytokines and exosomes are known to be released from MDSCs and play a role in intercellular communications[10, 44], we further tested whether exosomes released from DOX-MDSCs have a role in the induction of new blood vessels and suppression of T cell activation. Exosomes released from the VEH-MDSCs and DOX-MDSCs were examined for tumor angiogenesis. An enhanced tube formation was observed in response to exosomes from DOX-MDSC when compared with

VEH-MDSC (Fig. 3A). The adhesion of circulating tumor cells to endothelial cells is an important event in determining metastasis. To investigate whether exosome treatment could alter the adhesive property of endothelial cells, endothelial cells were pretreated with exosomes and, after 6 hours, the adhesion of tumor cells was evaluated. Exosomes from DOX-MDSCs significantly enhanced the adhesion of tumor cells compared with exosomes from VEH-MDSCs (Fig. 3B). Next, we tested the effect of exosomes on tumor angiogenesis in vivo. Administration of exosomes from DOX-MDSC promotes angiogenesis, as evaluated by quantification of the number of endothelial cell-containing ($CD31^+$ and α-SMA^+) blood vessels (Fig. 3C).

To determine whether exosomes from DOX-MDSCs are suppressive to T cell activity, we co-cultured exosomes isolated from lung VEH-MDSCs, DOX-MDSCs or MDSCs with naïve T cells under Th1 cell culture conditions. Exosomes from DOX-MDSCs significantly suppressed Th1 cell proliferation and IFN-γ secretion more than exosomes from VEH-MDSCs (Supplementary Fig. **4**). To test whether DOX-MDSC-derived exosomes contribute to the induction of Th2 cell responses in vitro, $CD4^+$ T cells from OT-II transgenic mice were used. MDSC-derived exosomes were mixed with OT-II splenocytes in the presence of control or OT-II specific peptides, and cytokine production was evaluated. DOX-MDSC-derived exosomes displayed a potent ability to inhibit T cell proliferation (Fig. 3D). Furthermore, the addition of DOX-MDSC-derived exosomes significantly promoted the production of IL-4 and IL-13 (Fig. 3E–F). Collectively, these data indicate that MDSC-derived exosomes contribute to MDSC-mediated suppression of Th1 cell activation and DOX treatment enhanced the MDSC-derived exosomal suppression of T cell activity, tumor angiogenesis, and induced Th2 cell responses in the lung of tumor bearing mice.

Induction of MDSC exosomal miR-126a is regulated by DOX treatment

To further explore the molecular mechanisms underlying DOX-exosome mediated induction of Th2 cell responses, we first performed a miRNA microarray analysis of MDSC exosomes. Total exosomal RNA from DOX-MDSCs and VEH-MDSCs were extracted and miRNA expression profiling was performed. Among the exosomal miRNAs analyzed, 11 miRNAs from DOX-MDSCs were significantly altered compared with the VEH-MDSCs (significant at 0.01 level of the univariate test; Supplementary Fig. **5A**). We then focused on miRNAs that could potentially function as tumor angiogenesis factors and induce Th2 cell responses. Within the three most expressed miRs in the exosome microRNA profile, the level of miR-126a was much higher in DOX-MDSC exosomes than in VEH-MDSC exosomes (Supplementary Fig. **5A**). The results were confirmed by real-time PCR (Supplementary Fig. **5B**). In addition, the treatment of ex vivo cultured lung MDSCs with DOX led to induction of miR-126a in MDSCs and its derived exosomes (Supplementary Fig. **5C**). The treatment of MDSCs with GW4869 that was reported to inhibit the secretion of exosome from cells[8, 31] resulted in reduction of miR-126a secreted in the exosomes of the DOX-treated MDSC (Supplementary Fig. **5D**). miRNAs can be selectively or concentration dependent encapsulated in exosomes. We transfected DOX-MDSCs with miR-126a hairpin inhibitors, miR-126a mimic or a control inhibitor (scramble RNA, named mock) with a nanovector made of grapefruit derived lipids[49]. A miR-126a inhibitor treatment significantly reduced miR-126a expressed in MDSC and in MDSC-derived exosomes (Supplementary

Fig. **6A**) whereas transfection of miR126 mimic led to an increase in miR-126a encapsulated in the exosomes (Supplementary Fig. **6B**), suggesting that miR-126a is sorted into exosomes. Together, these data support that DOX induces miR-126a expression in MDSCs and subsequently is released from MDSCs via the exosomal biogenesis pathway.

To test whether MDSC miR-126a is transferred to ECs/CD4 T cells, MDSCs were transfected with fluorescent labeled miR-126 mimics, washed, and then co-cultured with ECs or CD4 T cells in a transwell assay. We observed after an overnight incubation that the fluorescent labeled miR-126a was transferred to the ECs (Supplementary Fig. **7A**) or CD4 T cells (Supplementary Fig. **7B**). We then examined whether DOX-induced miR-126a in MDSC or MDSC-derived exosomes contribute to the induction of Th2 cell responses and angiogenesis in vitro. Transfection of Th2-cell-polarized T cells with miR-126a mimic increased the expression of miR-126a and enhanced the secretion of IL-4 and IL-13 (Fig. 4A). In contrast, transfection of Th1-cell-polarized T cells with miR-126a mimic decreased the secretion of IFN-γ (Fig. 4B). These observations suggest that the transfer of miR-126a from MDSCs to T cells may be an important intermediary step for the induction of Th2 cells. To further test whether DOX-induced MDSC exosomes contribute to the suppression of Th1 cell responses, we co-cultured VEH-MDSC-derived or DOX-MDSC-derived exosomes with Th1 cells. The result of ELISA analysis indicated that DOX-MDSC-derived exosomes significantly suppress the induction of IFN-γ, whereas exosomes from miR-126a inhibitor-transfected MDSCs had lost their ability to suppress induction of IFN-γ (Fig. 4C). We further examined the effects of exosomes derived from miR-126a inhibitor-transfected and miR-126a mimic-transfected MDSCs on tube formation in vitro. Exosomes derived from miR-126a mimic-transfected MDSCs had an enhanced effect on tube formation (Fig. 4D), whereas exosomes from miR-126a inhibitor-transfected MDSCs had a substantially reduced effect on tube formation (Fig. 4D). These data indicate that DOX-induced exosomal miR-126a contributes to MDSC-exosome mediated induction of Th2 T cells, prompting angiogenesis.

miR-126a-S100A8/9 Axis is regulated by DOX-induced IL-33/IL-13

Our data showed that IL-33 was induced in lung tissue upon DOX treatment. To determine the effect of DOX-induced IL-33/IL-13 on miRNA expression in MDSC, we exposed lung MDSCs from naïve mice to IL-13 and/or IL-33 for 4 days in culture. Notably, the expression of miR-126a is significantly induced in MDSC by IL-13 and/or IL-33 (Fig. 5A). To examine the role of IL-13/IL-33 induced miR-126a in promoting MDSC accumulation and/or activation, lung MDSCs from 4T1-tumor bearing mice were transfected with miR-126a encapsulated in a grapefruit exosome-like nano-vector[49]. Real-time PCR results suggest that the expression of Arg1, S100A8 and S100A9 were increased due to miR-126a transfection (Supplementary Fig. **8**). Conversely, lung MDSCs from 4T1 tumor bearing mice transfected with miR-126a inhibitor have a decreased expression of S100A8 and S100A9 (Supplementary Fig. **8**). High levels of S100A8/9 in $CD11b^{+}Gr1^{+}$ myeloid cells have been reported to be correlated with lung metastases in patients with breast cancer[1]. Importantly, MDSC-derived S100A8/9 can enhance cancer cell survival, which might be linked to chemo resistance. Indeed, when naïve MDSCs were exposed to DOX for 48 hours, exosomes from the miR-126a-transfected cells increased the survival of MDSC response to DOX treatment

compared with exosomes from cells transfected with scramble miRNA (Fig. 5B). The role of miR-126a in rescuing MDSCs from death was further supported by the fact that exosomes from MDSCs transfected with miR-126a inhibitor induced more MDSCs death (Fig. 5B). These data indicate that DOX-induced miR-126a may also have a role in regulating survival pathway(s) in MDSCs. To determine whether the observed miR-126a mediated up-regulation of S100A8 and S100A9 was associated with MDSC accumulation, we generated MDSCs that overexpressed miR-126a with/without knockdown of S100A8, S100A9, or both (S100A8/9) and evaluated differentiation of myeloid cells in the presence of GM-CSF. Overexpression of miR-126a significantly reduced the differentiation of DCs and substantially increased the production of Gr-1^{+}CD11b^{+} MDSCs compared with control (Fig. 5C). In contrast, knockdown of S100A9 did appreciably prevent the inhibition of the differentiation and survival of myeloid cells with overexpression of miR-126a (Fig. 5C–5D). Collectively, these data suggest that S100A9 is one of the miR-126a regulated genes in terms of regulation of MDSC differentiation and survival.

Systemic delivery of miR-126a inhibitor enhances DOX therapeutic effect on anti-lung metastasis

We have recently developed grapefruit-derived nanovectors (GNVs) capable of encapsulating siRNAs[49]. To address whether this edible plant-derived nanovector could be used to target MDSCs in tumor models, 4T1 tumor-bearing mice were administered i.v. PKH26-labeled GNVs carrying miR-126a. 12 h after administration, we observed the monocytic MDSCs (CD11b^{+}Ly6G^{-}Ly6C^{+}) in the blood (15.9%), lung (14.9%), spleen (13.6%) and liver (21.6%) were GNV^{+} by flow cytometry (Supplementary Fig. **9**). These data indicate that GNVs delivered miRNA efficiently to local and systemic MDSCs in vivo.

We next investigated the effects of miR-126a delivery on lung metastasis in breast tumor development. 4T1 Tumor-bearing mice were i.v. injected with GNVs, GNVs carrying miR-126a inhibitor, or GNVs carrying miR-126a mimic at a dose of 1.5 mg/kg twice each week for 4 wks. miR-126a inhibitor in combination with DOX treatment resulted in a modest decrease in mammary tumor volume compared with DOX and GNV treated control mice (Fig. 6A). However, the number of metastases induced by tumor cells was very low in mice injected with GNV-miR-126a inhibitor; whereas, a significant increase in the number of metastatic nodules in the lungs was observed in mice treated with GNV-miR-126a mimic (Fig. 6B–C).

To evaluate whether the administration of GNV-miR-126a inhibitor or mimic modified the lung microenvironment, the expression of VEGF, MMP9, and MMP2 was studied. The enhanced expression of MMP9 and VEGF in lung after treatment with GNV-miR-126a-mimic was evident by immunohistochemistry (Fig. 6D). qRT-PCR further confirmed GNV-miR-126a inhibitor or but not mimic, significantly decreased VEGF, MMP2, and MMP9 expression in total lung tissue (Supplementary Fig. **10A**). Furthermore, the proangiogenetic effect of GNV-miR-126a-mimic was significantly greater in vivo than that of GNV-miR-126a inhibitor (Fig. 6D). Together, these results provide compelling evidence that delivery of GNV-miR-126a inhibitor suppresses lung metastasis during breast tumor development by reducing local vascular growth after DOX treatment.

Fluorescent-activated cell sorting analysis of the predominant myeloid subtypes infiltrating lung revealed that in combination with GNV-miR-126a inhibitor, the recruitment of $CD45^+CD11b^+Gr\text{-}1^+F4/80^-$ MDSC was significantly decreased following treatment with DOX (Fig. 6E). These results were also supported by the fact that the frequency of $CD45^+CD11b^+Gr\text{-}1^+F4/80^-$ MDSC was significantly increased in DOX plus GNV-miR-126a mimic treated animals (Fig. 6E). However, analysis of myeloid subtypes remaining in tumor tissue following GNV-miR-126a inhibitor or GNV-miR-126a mimic treatment revealed no significant change in CD80, CD86, or MHCII expression (data not shown). In DOX-treated mice, delivery of GNV-miR-126a inhibitor suppressed the secretion of IL-4 and IL-13 from lung Th2 cells (Fig. 6F), with no effect on infiltration of NK cells, T regulatory cells or $CD8^+$ T cells (data not shown). In contrast, treatment with GNV-miR-126a mimic significantly promoted DOX-induced lung Th2 cell responses when compared to those treated with GNVs (Fig. 6F). The fact that miR-126a promotes Th2 cell responses and inhibits Th1 cell induction is further supported by FACS analysis data indicating that GNV-miR-126a inhibitor treatment showed increased expression of T-bet and decreased expression of GATA3 (Supplementary Fig. **10B**).

Discussion

MDSCs have emerged as an immunosuppressive-associated cell and are increasingly associated with disease aggressiveness, poor prognosis, drug resistance and metastasis. In this study, we determined the metastatic effects of exosomes released from MDSCs in DOX-treated mice and investigated the mechanisms mediating these effects. While doxorubicin treatment was largely efficacious in inhibiting primary tumors, it significantly increased the incidence and burden of pulmonary metastasis by miR-126a$^+$MDSC exosomes. Induction of miR-126a$^+$ MDSC exosomes by doxorubicin strongly increased the expression of inflammatory cytokine IL-13, which is released from Th2 cells in the lungs. These proinflammatory changes promoted the outgrowth of both MDSCs and Th2 cells in the lung where they increased blood vessel formation and promote lung metastasis of breast cancer via MDSC exosomal miR-126a. These results suggest that doxorubicin therapy of cancer patients may activate inflammatory circuits that promote angiogenesis and metastasis, at premetastatic niches where invasion occurs in distant organs through induction by miR-126a$^+$ MDSC exosomes. Taken together, our findings suggest that efforts to target miR-126a$^+$ MDSC exosome production and/or the exosomal releasing pathway may simultaneously quell inflammatory pathways that promote malignant progression, with implications for how to prevent tumor recurrence and the establishment of metastatic lesions, either during chemotherapy or after it is completed.

In this study, the finding that DOX-induced exosomal miR-126a contributes to developing DOX therapy resistance provides a foundation for further identifying the molecular pathway(s) underlying how DOX induces miR-126a through IL-13 receptor expression on MDSCs and molecules targeted by exosomal miR-126a on the MDSC exosome recipient cells. Furthermore, the results show that anti-miR-126a therapy as demonstrated in this study prevents chemotherapy resistance by targeting MDSCs, implying that this strategy could be beneficial for treatment of cancer patients in combination with chemotherapy.

In addition, finding that an increase in miR-126a^{+}MDSC exosomes is associated with chemotherapy resistance could be utilized to predict whether DOX should be used for treatment. It is anticipated that circulating miR-126a^{+}MDSC exosomes in plasma and/or serum are high in the cancer patients who are intrinsically resistant or acquired resistant to DOX treatment. Therefore, this finding has potential utility as diagnostic, prognostic, and predictive biomarkers for determining chemotherapy susceptibility.

As summarized in Supplementary figure 11, we propose a new mechanism that promotes lung metastatic progression through the crosstalk between MDSC-derived exosomes, Th2 cells, and endothelial cells. Our data identify MDSC exosome-mediated transfer of the miR-126a as a key regulator of activation of Th2 cells and endothelial cells and metastatic progression.

In this study, we used an anti-sense of miR126a approach to specifically block the effect of miR126a. Myeloid specific miR126 knockout mice could be used to address this issue however these mice are not commercially available. However, one would need to be cautious because knockout of myeloid miR126a may have unpredictable effects on the myeloid cells, from development, differentiation to maturation of myeloid cells. Proteins encoded by these mRNAs may play a role in sorting the factors that regulate the functions of Th2 T cells and endothelial cells into MDSC exosomes.

It is well-known that immune cell derived exosomes also communicate with tumor cells. In this study, we show that MDSCs communicated with T cells and endothelial cells through MDSC exosomes. This finding provides a foundation for future studies to determine whether MDSC exosome miR-126a induced by DOX has an effect on cancer cells and contributes to the cancer cells developing chemo resistance.

Our result show that among of MDSC exosomes miRNAs, miR126a is one of miRNAs induced by DOX treatment and one of the most enriched miRNAs in MDSC exosomes. Some published[30] data suggest that miRNAs are not randomly incorporated into exosomes. These studies show that parent cells possess a sorting mechanism that guides specific intracellular miRNAs to enter exosomes. Although the mechanisms underlying sorting miRNA into exosomes remains largely unclear, some cellular machinery involved in this sorting is: sphingomyelinase 2 (nSMase2)-dependent[23]; the miRNA motif and sumoylated heterogeneous nuclear ribonucleoproteins (hnRNPs)-dependent pathway[46]; and the 3′-end of the miRNA sequence-dependent pathway[22].

It is well known that mature miRNAs can interact with assembly proteins to form a complex called miRISC. The main components of miRISC include miRNA, miRNA-repressible mRNA, GW182, and AGO2. Recent studies recognized a possible correlation between AGO2 and exosomal miRNA sorting. Knockout of AGO2 could decrease the types or abundance of the preferentially-exported miRNAs in exosomes[19]. In summary, specific sequences present in certain miRNAs may guide their incorporation into exosomes, whereas some enzymes or other proteins may control sorting of exosomal miRNAs as well, in a miRNA sequence-independent fashion. Yet to be determined is whether Dox induced proteins are involved in sorting miR126a into MDSC exosomes. Identification of such

proteins could open up new avenue for developing therapeutic strategies for reversing MDSC exosome mediated immunotherapy.

Material and Methods

Animals and treatments

C57BL/6J and OT-II mice in a C57BL/6 background and BALB/c, Rag1$^{-/-}$ mice in a BALB/c background were obtained from Jackson Laboratories. All animal procedures were approved by the University of Louisville Institutional Animal Care and Use Committee.

Reagents, antibodies and flow cytometry

Mouse miR-126a mimic (catalogue # MI0000153) and miR-126a inhibitor (anti-sense of miR126a, 5'-CGCGUACCAAAAGUAAUAAUG-3′) were purchased from Dharmacon. Doxorubicin, paclitaxel and 5-fluorouracil were purchased from Sigma-Aldrich. Recombinant murine IL-33 (rmIL-33) was obtained from Biolegend. Mouse IL-33 mAb (Clone 396118) and isotype control were purchased from R&D Systems. For analysis of surface markers, cells were stained in PBS containing 2% (wt/vol) BSA. Intracellular staining of the transcription factors Foxp3 was performed using the Foxp3 Fix/Perm Buffer Set (eBioscience). For detection of intracellular cytokines, cells were first stimulated for 4 h with 50 ng/ml PMA and 1μg/ml ionomycin in the presence of Brefeldin A (5μg/ml; All obtained from Sigma), followed by staining for surface markers. Cells were then fixed and permeabilized using the Foxp3 Fix/Perm Buffer Set (eBioscience) and stained for intracellular cytokines. The following antibodies were used at a dilution of 1/200–1/600: PerCP-Cy5.5, PE-, FITC- or APC-labeled anti-IL-13 (eBio13A, eBioscience), PE- or APC-labeled anti-IL-4 (11B11, eBioscience), APC- or PE-Cy7-labeled anti-IFN (XMG1.2), PE-labeled anti-Foxp3 (FJK-16s, eBioscience), PE-, FITC- or APC-labeled anti-CD11b (M1/70), PE-, FITC- or APC-labeled anti-CD4 (RM4-5), PE-Cy7-labeled anti-CD3 (145-2C11), FITC-, PerCP-Cy5.5 or Pacific Blue-labeled anti-CD45 (30-F11), PE-anti-Gr-1 (RB6-8C5), PE- or FITC-labeled anti-mouse Ly6G (1A8). All antibodies were obtained from Biolegend unless otherwise noted. Flow cytometry data were acquired on a 5-color FACScan (Becton Dickinson) and analyzed using FlowJo software (Treestar). Cell sorting was performed using a FACSAria II.

Histology and immunohistochemistry

Tissue specimens were fixed in 10% formalin, dehydrated, and then embedded in paraffin. Tissue samples were cut at 5 μm thicknesses and stained with hematoxylin and eosin. For immunofluorescence analysis, tissue sections were subjected to antigen retrieval by boiling the slides in Antigen Unmasking Solution (Vector Laboratories) for 10 minutes according to instructions. Sections were then blocked for 1 hour at 22°C with 5% BSA in PBS and incubated overnight at 4°C with the primary antibodies, i.e., rabbit polyclonal VEGF, MMP9 from Santa Cruz Biotechnology Inc [Santa Cruz, CA] used at a dilution of 1/50, mouse monoclonal anti-E-cadherin, anti-vimentin, CD31 and CD11b were purchased from BD Bioscience (San Jose, CA) and used at a dilution of 1/100. Primary antibodies were detected by Alexa Fluor 488, 594 or 647 conjugated goat anti-mouse, anti-rabbit IgG and anti-rat (1:600, Invitrogen). Tissues were counterstained with DAPI and images were captured on a

Zeiss LSM 510 confocal microscope equipped with a digital image analysis system (Pixera). For immunofluorescence analysis of macrophages, OCT (Sakura Finetek)-embedded tissue cryosections (9μm-thick) were stained with F4/80 (BM8, ebioscience).

RNA extraction and PCR

Total RNA was isolated from the lung, liver and spleen lymphocytes or 4T1 tumor cells using the Qiagen RNeasy RNA isolation Kit and was used to synthesize cDNA. RNA (1μg) was reverse-transcribed with Superscript III and random primers (Invitrogen). For quantitation of genes of interest, cDNA samples were amplified in a CFX96 Realtime System (Bio-Rad Laboratories, Hercules, CA, USA) and SYBR Green Master Mix (Invitrogen) and specific primers (Supplemental Table 1) according to the manufacturer's instructions. Fold changes in mRNA expression between treatments and controls were determined by the δCT method as described[52]. Differences between groups were determined using a two-sided Student's *t*-test and one-way ANOVA. Error bars on plots represent ± SEM, unless otherwise noted. The data were normalized to a GAPDH reference. All primers were purchased from Eurofins MWG Operon.

ELISA

The quantity of IL-4, IL-33, sST2, IL-13, IFN-γ (eBioscience), CXCL1, CXCL2 and CCL2 (R&D Systems) were determined in culture supernatants, serum and tissue using ELISA kits according to the manufacturer's instructions. The sensitivity of the assay was <20 pg/ml.

Cells and cell culture conditions

Breast cancer cell line 4T1, E0771, MDA-MB-231 and the murine endothelial cell line 2H11 were purchased from ATCC and maintained in DMEM supplemented with 10% fetal bovine serum (FBS) and 100 U/ml penicillin/streptomycin. All cells were grown in a humidified atmosphere of 5% CO_2 at 37°C.

For MDSC and MDSC derived exosome-mediated Th1/Th2 proliferation and differentiation, naïve $CD4^+CD25^-CD62L^+$ T lymphocytes were cultured for 5 days with anti-CD3 (5μg/ml, 2C11, Bio X cell), anti-CD28 (2μg/ml, 37.51; Bio X Cell), IL-2 (10ng/ml), anti-IL-4 (10μg/ml, for Th1) or anti-IFN-γ (10μg/ml, for Th2) in the presence of exosomes (50μg/ml), followed by stimulation with PMA and ionomycin in the presence of brefeldin A (10μg/ml Sigma). Intracellular cytokine production on $CD4^+$ T cells was determined by flow cytometry. For MDSC-T cell co-cultures, 5×10^5 MDSCs and 2.5×10^5 OT-II T cells were mixed in the presence of cognate peptide (5 μg/ml; OVA) and/or exosomes (50μg/ml). After 4 d of culture, live T cells were collected and stimulated with PMA (phorbol 12-myristate 13-acetate, 50 ng/ml) and ionomycin (1μg/ml Sigma) plus brefeldin A (10μg/ml Sigma) for intracellular cytokine staining or for mRNA analysis. mRNA were assessed by RT-PCR and supernatants were used for cytokine measurement by ELISA.

MDSC survival assay

To address MDSC survival, 1×10^6 MDSCs were plated in a 12 well plate. Cells were untreated, treated with 20nM doxorubicin in the presence of exosomes derived from MDSC

transfected with 100 nM miR-126a inhibitor (anti-sense of miR126a), 100 nM mimic or mock (scramble miRNA). Viability and cell number were determined by propidium iodide exclusion or with Calcein Dyes (eBioscience) for staining live cells.

Exosomes isolation

For preparation of tumor exosomes, 4T1 cells was cultured in vitro at 37°C in a humidified 5% CO_2 atmosphere in air in complete medium (DMEM with 5% FCS that had been ultracentrifuged for 16 h at 100,000 g to exclude bovine exosomes). The exosomes were purified from the supernatants by differential centrifugation. In brief, cells were removed by centrifugation for 10 min at 300 g. Supernatants were collected and centrifuged sequentially twice for 10 min at 500 g, once for 15 min at 2,000 g, once for 30 min at 10,000 g, and once for 60 min at 100,000 g. Pelleted exosomes were resuspended in 5 ml of 2.6 M sucrose, 20 mM Tris-HCl (pH 7.2), and floated into an overlaid linear sucrose gradient (2.0–0.25 M sucrose, 20 mM Tris-HCl (pH 7.2)) in an SW41 tube for 16 h at 270,000 g. For preparation of MDSC exosomes, $CD11b^{+}Gr\text{-}1^{+}$MDSC were sorted by FACS from spleen, lung or tumor and cultured for 3 days in the presence of 1ng/ml GM-CSF. The supernatants containing the exosomes produced by MDSCs were then harvested. Cell supernatant was centrifuged at 300g for 10 minutes. Cell-free supernatant was further centrifuged at 2,000g and then 10,000g to remove dead cells and cell debris. Pelleted exosomes were collected after 90 min centrifuge at 100,000 gmax. In some experiments, exosomes were also purified using Exosome Isolation Reagent (Invitrogen). For blocking of exosome release from MDSCs, sorted MDSCs were treated with GW-4869 (10μM) for 48h in the presence of 1 ng/ml GM-CSF.

In vivo tumor growth, chemotherapy and metastatic assays

Female wild type BALB/c mice (4T1 model) or C57BL/6J mice (E0771 model), 6 to 8 weeks old, were obtained from The Jackson Laboratory (Bar Harbor, ME). 1.5×10^5 4T1 cells or 1×10^6 E0771 cells were injected in the mammary fat pads of mice in a volume of 50μl of PBS. Ten days after tumor injection (tumor size, 100–120 mm^3), mice were administered doxorubicin (5 mg/kg; intravenously), paclitaxel (20mg/kg) or control PBS twice weekly for six doses. Spleens, lung, liver, blood and tumors were collected and analyzed for the presence of MDSCs at 14, 17, 24 and 30 days after tumor cell injection. For evaluating the effects of doxorubicin plus delivery of GNV-miRNA combination therapy, 10-day tumor bearing mice with the same tumor size were randomly divided into three groups (n =7), and were I.V. injected with doxorubicin (5mg/kg) plus scramble miRNA, or miR-126a inhibitor or miR-126a mimic (1.5 mg/kg of body weight) delivered by GNVs twice weekly for eight doses. For CT26 tumor induction, 2×10^5 CT26-LUC cells in 50 μL 1×PBS were injected subcutaneously in the shaved right flank. When the tumor had grown to 0.1–0.2 cm, mice were injected i.p. with 5-fluorouracil (50mg/kg; intraperitoneally) twice weekly for six doses. To generate a mouse tumor metastasis model, 1×10^6 CT26-LUC cells per mouse were injected intravenously via the tail-vein.

Mice were euthanized for ethical reasons when they exhibited severe morbidity signs due to overwhelming metastatic lesions (endpoint at 6–7 weeks) in compliance with IACUC regulations. Based on our preliminary data, 7 mice per dose group for each treatment will

have 94% power and can detect a mean difference of 2.8 between treatment groups at each time point with a subject variance of 1 after controlling the overall type I error rate of 5% using analysis of variance (ANOVA). Mice were randomly divided into groups. Mice died within 72 hours after tumor cell injection were excluded from the evaluation. Tumors were measured every three days using calipers and calculated as $0.52\times\text{length}\times\text{width}^2$. Lungs were fixed in buffered formalde-fresh solution (Fisher) and stained with hematoxylin and eosin (H&E) for counting metastatic nodules.

Tube formation assay and adhesion assay

Matrigel (BD Biosciences) was added to the wells of a 48-well plate in a volume of 120 μl and allowed to solidify at 37°C for 30 min. After the matrigel solidified, endothelial cells (ECs) (4×10^4 per 0.2-ml well of a 48-well plate) were seeded in RPMI medium with 1% FBS with or without 50 μg/ml MDSC derived-exosomes at various concentrations for 16 h. Cell organization onto matrigel was analyzed using an inverted light microscope (Nikon). All tube-like structures were counted for each well; only closed networks of vessel-like tubes were counted. In some experiments ECs were co-incubated with different sources of MDSCs (1:1 ratio, each 2×10^4 per 0.2-ml well of a 48-well plate). MDSCs were sorted from lungs or tumors of tumor-bearing mice with or without chemotherapy treatment. The effect of MDSC derived exosomes on adhesion of 4T1 tumor cells to ECs was evaluated. EC monolayers were pretreated for 24 hours at 37°C in RPMI medium with 1% FCS with or without exosomes. 4T1 tumor cells (5×10^5 per well), labeled with CSFE, were added to the endothelial monolayer. The adhesion assay in static conditions was evaluated after 6 hours. After washings, cells adherent to ECs were counted by fluorescence microscopy (magnification×200) in 10 fields and expressed as mean ± SEM of cells per field.

Angiogenic Factor Assay

The presence of pro-/antiangiogenic factors in cell supernatants and cell lysates was assessed using the Proteome Profiler Antibody Array (R&D) specific for mouse angiogenesis. Sorted VEH-MDSC or DOX-MDSC from lung (2×10^6 cells, obtained by pooling five lung) were plated in DMEM and 2% FBS, and, after 5 d, their supernatants were collected and stored at −20 °C until analysis.

Exosomal miR-126a and myeloid cell differentiation

Bone marrow cells were harvested from the femurs and tibias of mice and sorted for progenitor cells (Lin^- c-Kit^+ $\text{CD11b}^-\text{Gr-1}^-$ cells). To assess the effects of MDSC-derived exosomes or miRNA on MDSC accumulation/DC differentiation, 1×10^6 enriched progenitor cells were placed into each well of 24-well plates for 5 days in 2-ml of RPMI supplemented with 10% FBS, 20 ng/ml GM-CSF, and 10 ng/ml IL-4 in the presence of GNVs carrying mock, miR-126a inhibitor or miR-126a mimic.

Isolation and uptake of exosome and GNVs trafficking *in vivo*

To isolate exosomes from cell culture medium, the cell culture supernatants were collected and purified by differential centrifugation using a previously described method[51]. To monitor exosome trafficking and uptake in vivo, exosomes or GNVs were labeled with the

PKH26 red fluorescent dye using a commercially available kit (Sigma-Aldrich) and according to a previously described protocol[50]. Tumor-bearing mouse received 40 μg PKH26-labeled exosomes administered intravenously via the tail-vein. Eighteen to twenty-four h after injection the mice were sacrificed and the peripheral blood and liver, lung, and spleen tissues were collected. Single-cell suspensions of each tissue were prepared in RPMI 1640 medium and subjected to FACS analysis. The percentages of cells containing exosomes or GNVs were determined by counting green fluorescent-positive cells.

Suppression assays

Naïve $CD4^+CD25^-CD62L^+$ T cells were labeled with 5mM CellTrace™ CFSE according to the manufacturer's instructions (Invitrogen) and stimulated with plate-bound anti-CD3 (5 μg/ml) and soluble CD28 (5 μg/ml) for 4 days in the presence or absence of exosomes (50μg/ml) from MDSC isolated from 4T1 tumor-bearing mice, treated or not with doxorubicin, at the following ratio, MDSC to T cell ratio= 1:2. After 4 days, cell proliferation was determined by measuring the dilution of CellTrace™ CFSE by flow cytometry after gating on the $CD4^+$ cell populations. The level and number of IFN-γ and CD4-producing cells in response to stimulation was evaluated by ELISA or FACS.

miRNA mimic and hairpin inhibitor transfection

MDSCs or bone marrow cells were cultured in 6-well plates and transfected the following day. 100 pmol miR-126a mimic or inhibitor encapsulated in grapefruit-derived nanovector (GNV)[49] was used. Cells were rested in exosome-free media, washed and co-cultured with T cells, as indicated, for 24–48 hours. Oligonucleotides with random sequence served as negative controls for miRNA mimic or inhibitor.

Statistical analysis

Values are shown as s.e.m. except otherwise indicated. Comparison of multiple experimental groups was performed by two-way Analysis of Variance test. A *t*-test was used to compare the means of two groups. *P* values of <0.05 were considered to be statistically significant. Sample sizes are calculated to allow significance to be reached.

Supplementary Material

Refer to Web version on PubMed Central for supplementary material.

Acknowledgments

This work was supported by grants from the National Institutes of Health (NIH) (R01AT008617, UH3TR000875) and the Louisville Veterans Administration Medical Center (VAMC) Merit Review Grants (to H.-G. Zhang). H.-G. Zhang is supported by a Research Career Scientist (RCS) Award, funded by the U.S. Department of Veterans Affairs. The authors thank Dr. Jerald Ainsworth for editorial assistance.

References

1. Acharyya S, Oskarsson T, Vanharanta S, Malladi S, Kim J, Morris PG, et al. A CXCL1 paracrine network links cancer chemoresistance and metastasis. Cell. 2012; 150:165–178. [PubMed: 22770218]

2. Agudo J, Ruzo A, Tung N, Salmon H, Leboeuf M, Hashimoto D, et al. The miR-126-VEGFR2 axis controls the innate response to pathogen-associated nucleic acids. Nature immunology. 2014; 15:54–62. [PubMed: 24270517]

3. Alizadeh D, Trad M, Hanke NT, Larmonier CB, Janikashvili N, Bonnotte B, et al. Doxorubicin eliminates myeloid-derived suppressor cells and enhances the efficacy of adoptive T-cell transfer in breast cancer. Cancer research. 2014; 74:104–118. [PubMed: 24197130]

4. Azmi AS, Bao B, Sarkar FH. Exosomes in cancer development, metastasis, and drug resistance: a comprehensive review. Cancer metastasis reviews. 2013; 32:623–642. [PubMed: 23709120]

5. Boelens MC, Wu TJ, Nabet BY, Xu B, Qiu Y, Yoon T, et al. Exosome transfer from stromal to breast cancer cells regulates therapy resistance pathways. Cell. 2014; 159:499–513. [PubMed: 25417103]

6. Bruchard M, Mignot G, Derangere V, Chalmin F, Chevriaux A, Vegran F, et al. Chemotherapy-triggered cathepsin B release in myeloid-derived suppressor cells activates the Nlrp3 inflammasome and promotes tumor growth. Nature medicine. 2013; 19:57–64.

7. Burke MC, Oei MS, Edwards NJ, Ostrand-Rosenberg S, Fenselau C. Ubiquitinated proteins in exosomes secreted by myeloid-derived suppressor cells. Journal of proteome research. 2014; 13:5965–5972. [PubMed: 25285581]

8. Chairoungdua A, Smith DL, Pochard P, Hull M, Caplan MJ. Exosome release of beta-catenin: a novel mechanism that antagonizes Wnt signaling. The Journal of cell biology. 2010; 190:1079–1091. [PubMed: 20837771]

9. Challagundla KB, Wise PM, Neviani P, Chava H, Murtadha M, Xu T, et al. Exosome-mediated transfer of microRNAs within the tumor microenvironment and neuroblastoma resistance to chemotherapy. Journal of the National Cancer Institute. 2015; 107

10. Colombo M, Raposo G, Thery C. Biogenesis, secretion, and intercellular interactions of exosomes and other extracellular vesicles. Annual review of cell and developmental biology. 2014; 30:255–289.

11. Condamine T, Ramachandran I, Youn JI, Gabrilovich DI. Regulation of tumor metastasis by myeloid-derived suppressor cells. Annual review of medicine. 2015; 66:97–110.

12. de Leeuw DC, Denkers F, Olthof MC, Rutten AP, Pouwels W, Schuurhuis GJ, et al. Attenuation of microRNA-126 expression that drives CD34+38- stem/progenitor cells in acute myeloid leukemia leads to tumor eradication. Cancer research. 2014; 74:2094–2105. [PubMed: 24477595]

13. Diaz-Montero CM, Salem ML, Nishimura MI, Garrett-Mayer E, Cole DJ, Montero AJ. Increased circulating myeloid-derived suppressor cells correlate with clinical cancer stage, metastatic tumor burden, and doxorubicin-cyclophosphamide chemotherapy. Cancer immunology, immunotherapy : CII. 2009; 58:49–59. [PubMed: 18446337]

14. Ebrahimi F, Gopalan V, Wahab R, Lu CT, Anthony Smith R, Lam AK. Deregulation of miR-126 expression in colorectal cancer pathogenesis and its clinical significance. Experimental cell research. 2015

15. Garlanda C, Anders HJ, Mantovani A. TIR8/SIGIRR: an IL-1R/TLR family member with regulatory functions in inflammation and T cell polarization. Trends in immunology. 2009; 30:439–446. [PubMed: 19699681]

16. Ghiringhelli F, Apetoh L. The interplay between the immune system and chemotherapy: emerging methods for optimizing therapy. Expert review of clinical immunology. 2014; 10:19–30. [PubMed: 24308838]

17. Goerke SM, Kiefer LS, Stark GB, Simunovic F, Finkenzeller G. miR-126 modulates angiogenic growth parameters of peripheral blood endothelial progenitor cells. Biological chemistry. 2015; 396:245–252. [PubMed: 25473802]

18. Guabiraba R, Besnard AG, Menezes GB, Secher T, Jabir MS, Amaral SS, et al. IL-33 targeting attenuates intestinal mucositis and enhances effective tumor chemotherapy in mice. Mucosal immunology. 2014; 7:1079–1093. [PubMed: 24424522]

19. Guduric-Fuchs J, O'Connor A, Camp B, O'Neill CL, Medina RJ, Simpson DA. Selective extracellular vesicle-mediated export of an overlapping set of microRNAs from multiple cell types. BMC genomics. 2012; 13:357. [PubMed: 22849433]

20. Joshi BH, Puri RK. IL-13 receptor-alpha2: a novel target for cancer therapy. Immunotherapy. 2009; 1:321–327. [PubMed: 20635949]

21. Koch R, Aung T, Vogel D, Chapuy B, Wenzel D, Becker S, et al. Nuclear trapping through inhibition of exosomal export by indomethacin increases cytostatic efficacy of doxorubicin and pixantrone. Clinical cancer research : an official journal of the American Association for Cancer Research. 2015
22. Koppers-Lalic D, Hackenberg M, Bijnsdorp IV, van Eijndhoven MA, Sadek P, Sie D, et al. Nontemplated nucleotide additions distinguish the small RNA composition in cells from exosomes. Cell reports. 2014; 8:1649–1658. [PubMed: 25242326]
23. Kosaka N, Iguchi H, Yoshioka Y, Takeshita F, Matsuki Y, Ochiya T. Secretory mechanisms and intercellular transfer of microRNAs in living cells. The Journal of biological chemistry. 2010; 285:17442–17452. [PubMed: 20353945]
24. Lieberman J, Slack F, Pandolfi PP, Chinnaiyan A, Agami R, Mendell JT. Noncoding RNAs and cancer. Cell. 2013; 153:9–10. [PubMed: 23781554]
25. Lin S, Gregory RI. MicroRNA biogenesis pathways in cancer. Nature reviews Cancer. 2015; 15:321–333. [PubMed: 25998712]
26. Marvel D, Gabrilovich DI. Myeloid-derived suppressor cells in the tumor microenvironment: expect the unexpected. The Journal of clinical investigation. 2015; 125:3356–3364. [PubMed: 26168215]
27. Mattes J, Collison A, Plank M, Phipps S, Foster PS. Antagonism of microRNA-126 suppresses the effector function of TH2 cells and the development of allergic airways disease. Proceedings of the National Academy of Sciences of the United States of America. 2009; 106:18704–18709. [PubMed: 19843690]
28. Meister J, Schmidt MH. miR-126 and miR-126*: new players in cancer. The Scientific World Journal. 2010; 10:2090–2100. [PubMed: 20953557]
29. Meyer C, Cagnon L, Costa-Nunes CM, Baumgaertner P, Montandon N, Leyvraz L, et al. Frequencies of circulating MDSC correlate with clinical outcome of melanoma patients treated with ipilimumab. Cancer immunology, immunotherapy : CII. 2014; 63:247–257. [PubMed: 24357148]
30. Ohshima K, Inoue K, Fujiwara A, Hatakeyama K, Kanto K, Watanabe Y, et al. Let-7 microRNA family is selectively secreted into the extracellular environment via exosomes in a metastatic gastric cancer cell line. PloS one. 2010; 5:e13247. [PubMed: 20949044]
31. Ohshima K, Kanto K, Hatakeyama K, Ide T, Wakabayashi-Nakao K, Watanabe Y, et al. Exosome-mediated extracellular release of polyadenylate-binding protein 1 in human metastatic duodenal cancer cells. Proteomics. 2014; 14:2297–2306. [PubMed: 25065644]
32. Ozkok A, Edelstein CL. Pathophysiology of cisplatin-induced acute kidney injury. BioMed research international. 2014; 2014:967826. [PubMed: 25165721]
33. Payne KK, Zoon CK, Wan W, Marlar K, Keim RC, Kenari MN, et al. Peripheral blood mononuclear cells of patients with breast cancer can be reprogrammed to enhance anti-HER-2/neu reactivity and overcome myeloid-derived suppressor cells. Breast cancer research and treatment. 2013; 142:45–57. [PubMed: 24197563]
34. Ran S. The Role of TLR4 in Chemotherapy-Driven Metastasis. Cancer research. 2015; 75:2405–2410. [PubMed: 25998620]
35. Reichenbach DK, Schwarze V, Matta BM, Tkachev V, Lieberknecht E, Liu Q, et al. The IL-33/ST2 axis augments effector T-cell responses during acute GVHD. Blood. 2015; 125:3183–3192. [PubMed: 25814531]
36. Rutkowski MR, Stephen TL, Svoronos N, Allegrezza MJ, Tesone AJ, Perales-Puchalt A, et al. Microbially driven TLR5-dependent signaling governs distal malignant progression through tumor-promoting inflammation. Cancer cell. 2015; 27:27–40. [PubMed: 25533336]
37. Schmieder A, Multhoff G, Radons J. Interleukin-33 acts as a pro-inflammatory cytokine and modulates its receptor gene expression in highly metastatic human pancreatic carcinoma cells. Cytokine. 2012; 60:514–521. [PubMed: 22819319]
38. Schober A, Nazari-Jahantigh M, Wei Y, Bidzhekov K, Gremse F, Grommes J, et al. MicroRNA-126-5p promotes endothelial proliferation and limits atherosclerosis by suppressing Dlk1. Nature medicine. 2014; 20:368–376.

39. Seidelin JB, Rogler G, Nielsen OH. A role for interleukin-33 in T(H)2-polarized intestinal inflammation? Mucosal immunology. 2011; 4:496–502. [PubMed: 21613987]
40. Shen J, Hung MC. Signaling-mediated regulation of MicroRNA processing. Cancer research. 2015; 75:783–791. [PubMed: 25660948]
41. Shibayama Y, Kondo T, Ohya H, Fujisawa S, Teshima T, Iseki K. Upregulation of microRNA-126-5p is associated with drug resistance to cytarabine and poor prognosis in AML patients. Oncology reports. 2015; 33:2176–2182. [PubMed: 25759982]
42. Suzuki A, Leland P, Joshi BH, Puri RK. Targeting of IL-4 and IL-13 receptors for cancer therapy. Cytokine. 2015; 75:79–88. [PubMed: 26088753]
43. Talmadge JE, Gabrilovich DI. History of myeloid-derived suppressor cells. Nature reviews Cancer. 2013; 13:739–752. [PubMed: 24060865]
44. Thery C, Ostrowski M, Segura E. Membrane vesicles as conveyors of immune responses. Nature reviews Immunology. 2009; 9:581–593.
45. Umansky V, Sevko A. Overcoming immunosuppression in the melanoma microenvironment induced by chronic inflammation. Cancer immunology, immunotherapy : CII. 2012; 61:275–282. [PubMed: 22120757]
46. Villarroya-Beltri C, Baixauli F, Gutierrez-Vazquez C, Sanchez-Madrid F, Mittelbrunn M. Sorting it out: regulation of exosome loading. Seminars in cancer biology. 2014; 28:3–13. [PubMed: 24769058]
47. Volk-Draper L, Hall K, Griggs C, Rajput S, Kohio P, DeNardo D, et al. Paclitaxel therapy promotes breast cancer metastasis in a TLR4-dependent manner. Cancer research. 2014; 74:5421–5434. [PubMed: 25274031]
48. Wang J, Hendrix A, Hernot S, Lemaire M, De Bruyne E, Van Valckenborgh E, et al. Bone marrow stromal cell-derived exosomes as communicators in drug resistance in multiple myeloma cells. Blood. 2014; 124:555–566. [PubMed: 24928860]
49. Wang Q, Zhuang X, Mu J, Deng ZB, Jiang H, Zhang L, et al. Delivery of therapeutic agents by nanoparticles made of grapefruit-derived lipids. Nature communications. 2013; 4:1867.
50. Wang Q, Ren Y, Mu J, Egilmez NK, Zhuang X, Deng Z, et al. Grapefruit-Derived Nanovectors Use an Activated Leukocyte Trafficking Pathway to Deliver Therapeutic Agents to Inflammatory Tumor Sites. Cancer research. 2015; 75:2520–2529. [PubMed: 25883092]
51. Xiang X, Liu Y, Zhuang X, Zhang S, Michalek S, Taylor DD, et al. TLR2-mediated expansion of MDSCs is dependent on the source of tumor exosomes. The American journal of pathology. 2010; 177:1606–1610. [PubMed: 20802178]
52. Xiang Y, Ma N, Wang D, Zhang Y, Zhou J, Wu G, et al. MiR-152 and miR-185 co-contribute to ovarian cancer cells cisplatin sensitivity by targeting DNMT1 directly: a novel epigenetic therapy independent of decitabine. Oncogene. 2014; 33:378–386. [PubMed: 23318422]
53. Yang Z, Wang R, Zhang T, Dong X. MicroRNA-126 regulates migration and invasion of gastric cancer by targeting CADM1. International journal of clinical and experimental pathology. 2015; 8:8869–8880. [PubMed: 26464628]
54. Yin Y, Huang X, Lynn KD, Thorpe PE. Phosphatidylserine-targeting antibody induces M1 macrophage polarization and promotes myeloid-derived suppressor cell differentiation. Cancer immunology research. 2013; 1:256–268. [PubMed: 24777853]

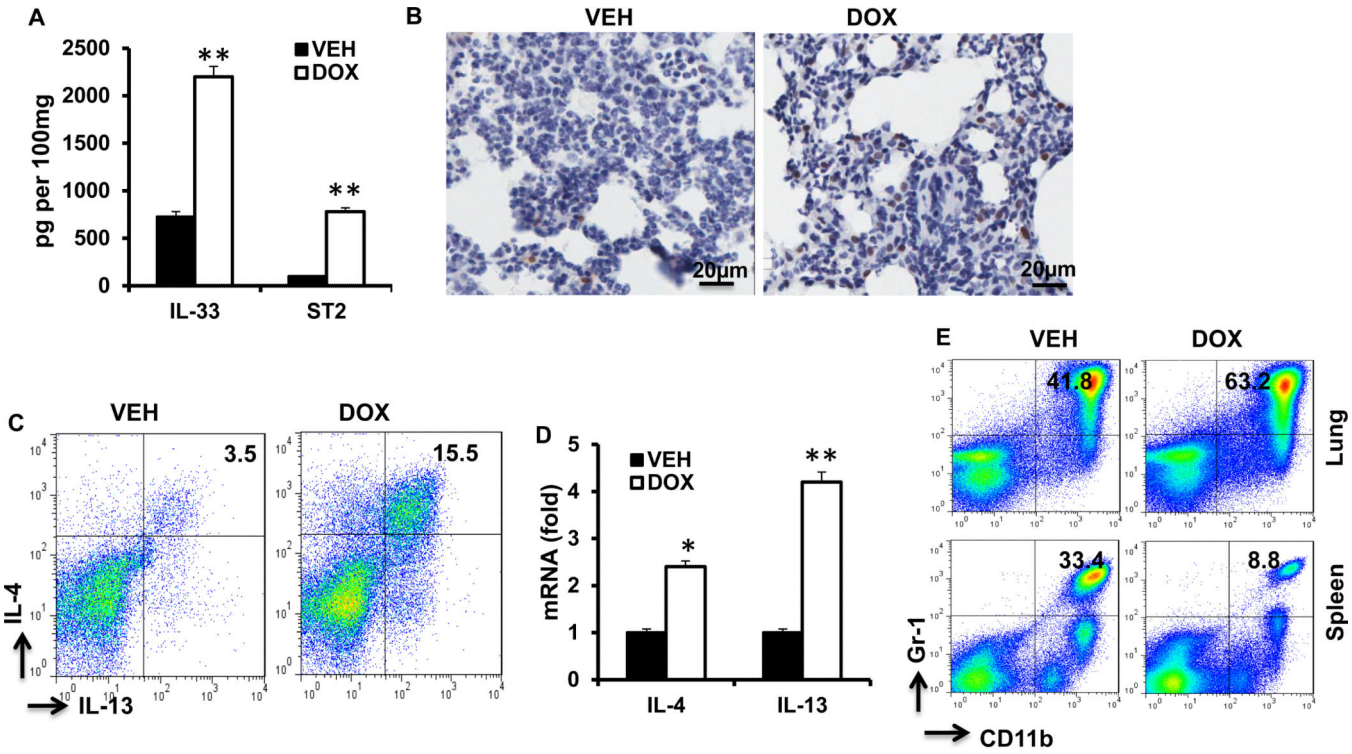

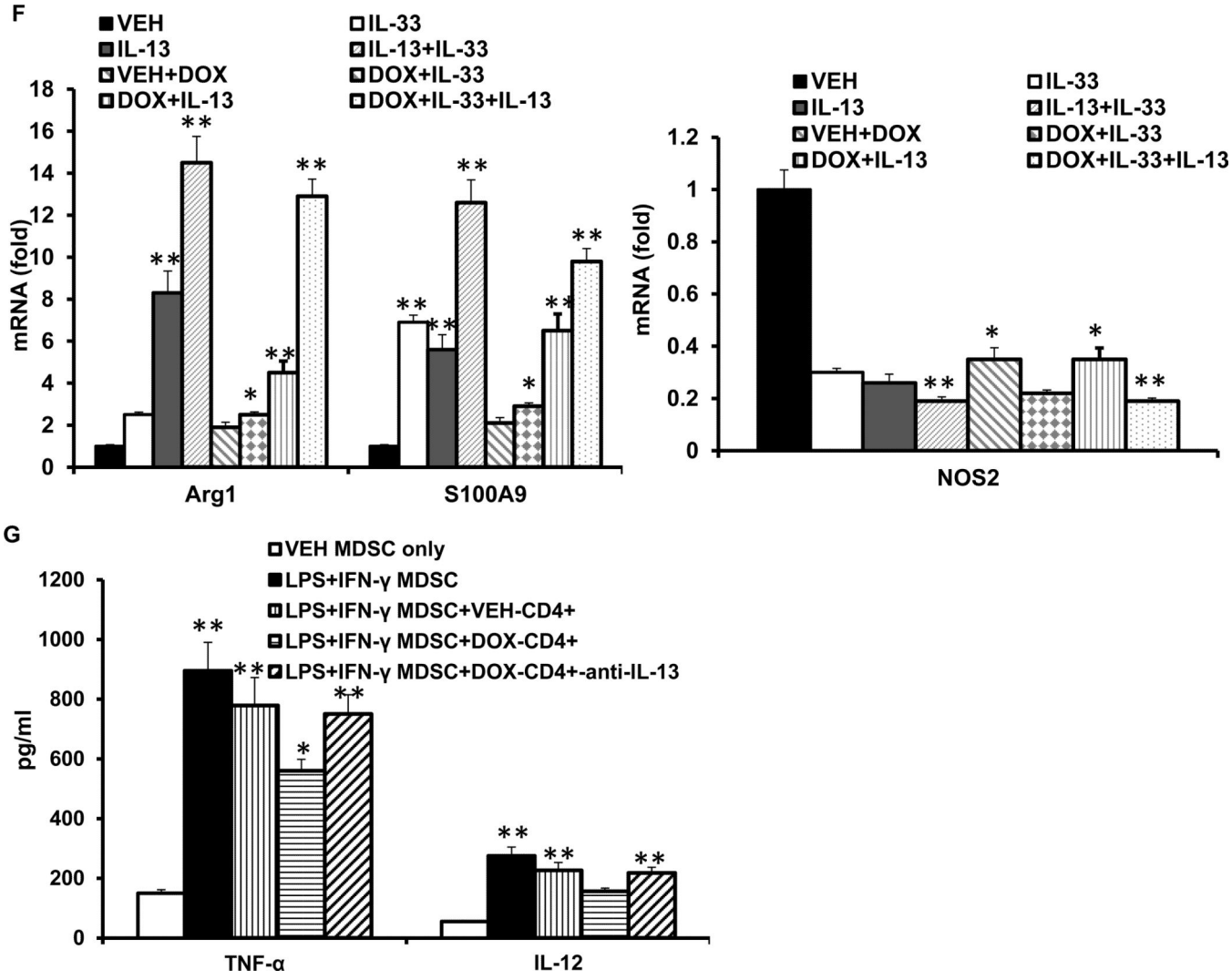

Figure 1. DOX induces a strong type-2 Immune response and the accumulation of MDSC in the lung

A) IL-33 or soluble ST2 concentrations in the lung of tumor-bearing mice after repeated injections of doxorubicin (5mg/kg) or vehicle were determined by ELISA; **B)** Representative immunohistochemical (IHC) staining for IL-33 in the lung of vehicle or DOX-treated tumor bearing mice. **C)** Lung cells from vehicle or DOX-treated tumor bearing mice (day 35) were restimulated with PMA and ionomycin and stained intracellularly for IL-4 and IL-13 on $CD4^+$ T cells. **D)** Real-time PCR for the expression of genes in $CD4^+$ T cells in lung from vehicle or DOX-treated tumor bearing mice. *P<0.05, **P<0.01 (Student's t-test). **E)** Proportion of MDSC $CD11b^+Gr\text{-}1^+$ in the spleen and lung of 4T1 tumor-bearing mice post-DOX treatment were examined by flow cytometry. **F**) Immature myeloid cells in the lung from naïve mice were stimulated with VEH, IL-13, IL-33 or IL-13 plus IL-33 in the absence or presence of Doxorubicin. Arg1, Nos2, and S100A9 mRNA expression was quantified by RT-PCR. **G**) DOX-induced $IL\text{-}13^+CD4^+$ T cells repress MDSC M1 phenotype. Untreated naïve $CD11b^+Gr1^+$ MDSC (VEH-MDSC) or IFN-γ (5 ng/ml) plus LPS (50 ng/ml)-treated MDSC (LPS+IFN-γ MDSC) were cultured with lung $CD4^+$ T cells sorted from vehicle

(VEH-CD4+) or DOX-treated (DOX-CD4+) tumor bearing mice in the presence or absence of anti-IL-13 antibody. The expression of TNF-α and IL-12 in conditioned medium evaluated by ELISA after 18 hr of co-culture. *P<0.05, **P<0.01 (Student's t-test).

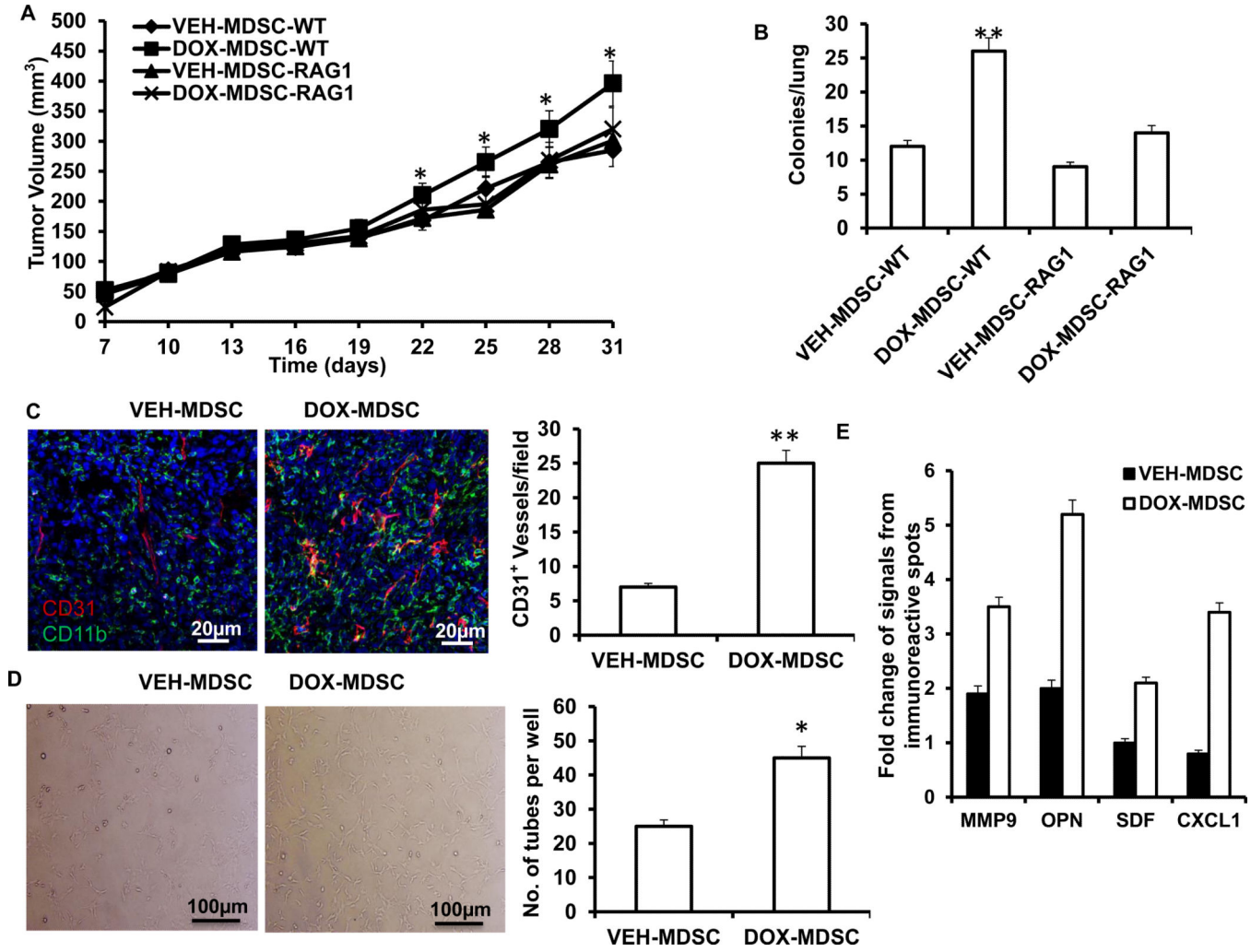

Figure 2. DOX-MDSC promote tumor growth

A) 2.5×10^5 4T1 cells and sorted 0.5×10^5 lung $CD11b^+Gr^+$ cells from vehicle or DOX-treated tumor bearing Balb/c mice or $Rag1^{-/-}$ mice were injected s.c. in Balb/c mice (n=7). Data are mean ± SEM. *$P < 0.05$. **B**) The number of lung colonies was examined. Data are mean ± SEM. **P<0.01 (Student's t-test). **C**) Immunohistochemical detection of CD31 (endothelial cells, red) and CD11b (myeloid cells, green) in 4T1 tumors. The number of $CD31^+$ blood vessels per field (mean ± SEM) averaged from 10 random fields are shown. Three tumors per each group were analyzed. Data are mean ± SEM. **P<0.01 (Student's t-test). (Scale bar, 20 μm). **D**) In vitro tube-formation assay. ECs were incubated with sorted $CD11b^+Gr^+$ cells from vehicle or DOX-treated tumor bearing mice. Images were taken after 18 h. Representative images are shown. The number of tube-like structures was counted per well of 48-well plates. Data are mean ± SEM of 3 independent experiments. *$P < 0.05$. **E**) Analysis of angiogenic proteins secreted by MDSC. Cells (1.5×10^6) were isolated by FACS from vehicle or DOX-treated tumor bearing mice and cultured for 5 d in DMEM, 2% FBS. The supernatants were then analyzed with the Mouse Angiogenesis Antibody Array Kit (R&D). Quantification of signals from immunoreactive spots is shown.

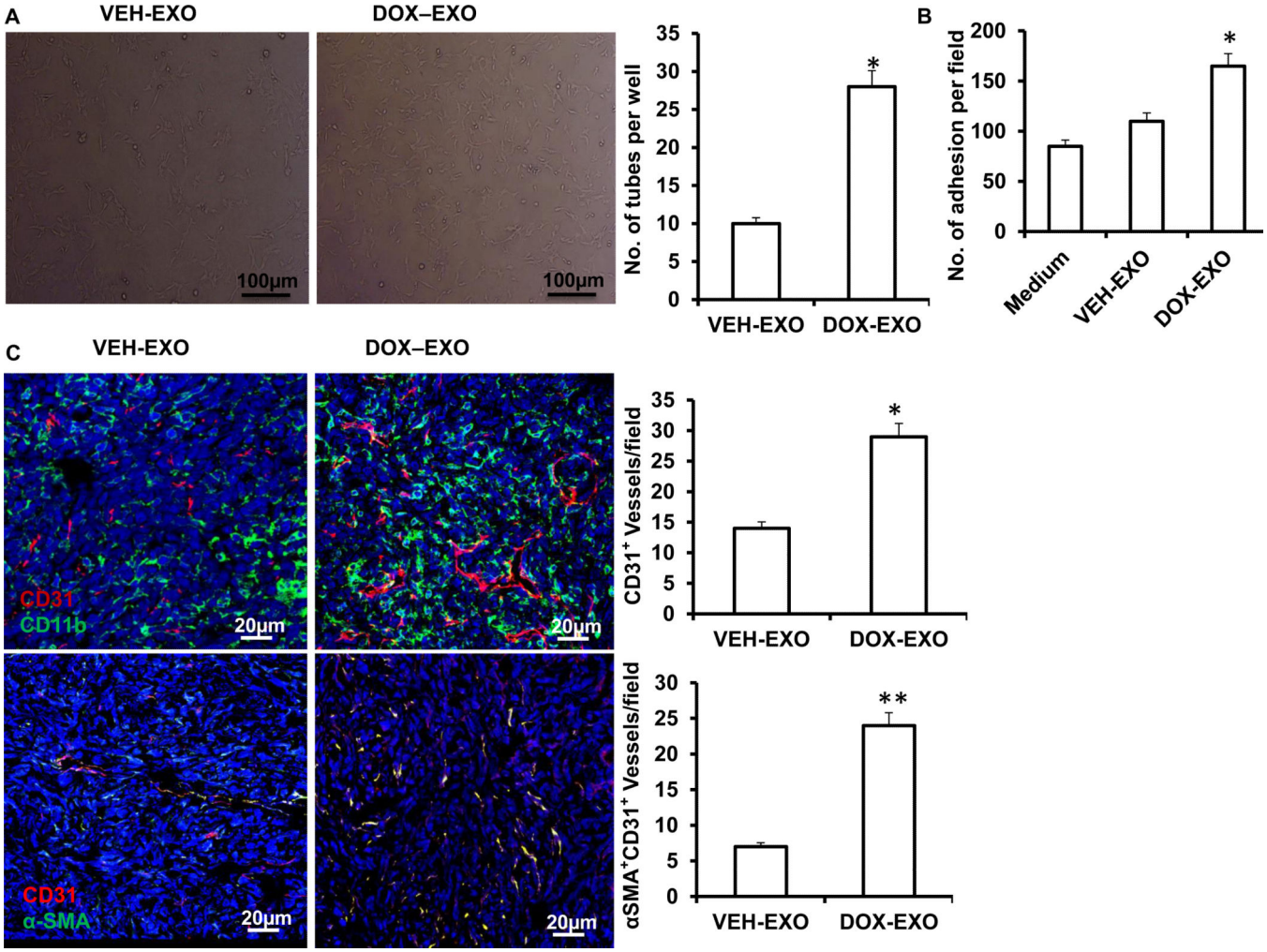

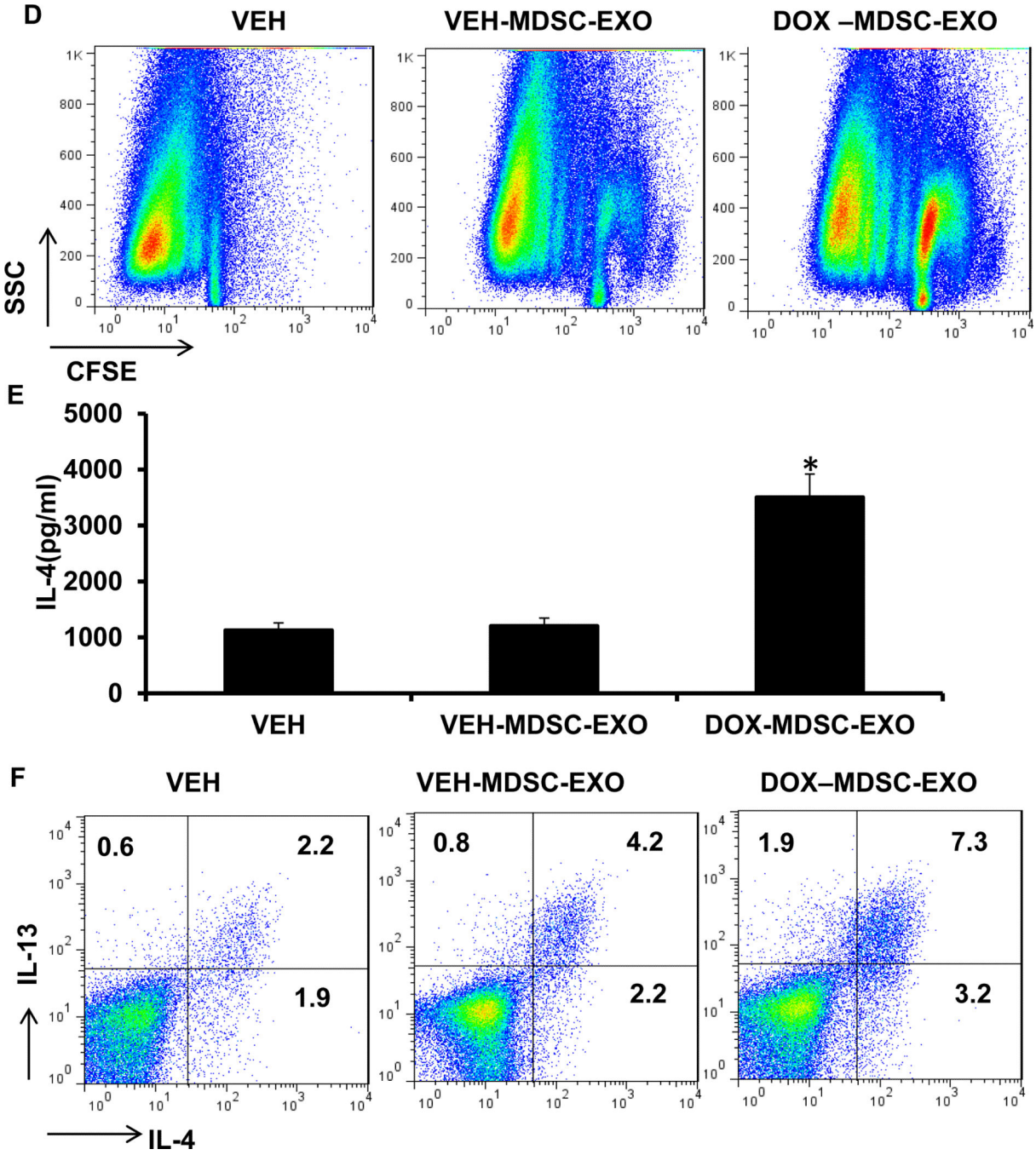

Figure 3. Exosomes derived from DOX-MDSCs regulate proangiogenic effects and T cells activity

A) In vitro tube-formation assay. ECs were incubated with (50μg/ml) exosomes from sorted VEH-MDSCs or DOX-MDSCs. Representative micrographs are shown. The number of tube-like structures was counted per well of 48-well plates. Data are mean ± SEM of 3 independent experiments. **P* < 0.05. **B**) Quantitative evaluation of adhesion of 4T1 tumor cells labeled with PKH26 dye to a monolayer of ECs unstimulated (RPMI) or stimulated with 50μg/ml of exosomes from MDSCs. Data are mean ± SEM. **P* < 0.05. **C**) In vivo

angiogenesis of MDSC exosomes. MDSC exosomes (200μg/ml) mixed with 2.5×10^5 4T1 cells were injected s.c. in BALB/c mice and repeatedly injected every three days. Mice were sacrificed 12 days after injection. Immunohistochemical detection of CD31 (red) and CD11b (green) or α-SMA (green) in 4T1 tumors were examined. The number of CD31+ blood vessels per field (mean ± SEM) averaged from 10 random fields are shown. *P<0.05, **P<0.01 (Student's t-test). **D–F**) CFSE-labeled OT-II $CD4^+$ T cells were co-cultured with VEH-MDSC- or DOX-MDSC-derived exosomes (50μg/ml) in the presence of 5μg/ml anti-CD3, 5μg/ml anti-CD28 and 10μg/ml anti-IFN-γ for 4 days. Proliferation of CFSE-labeled $CD4^+$ T cells (D), the level of IL-4 (E) in the supernatant of co-cultured cells, and the intracellular staining of IL-4 and IL-13 on $CD4^+$ T cells (F) were determined. Data are mean ± SEM. *P<0.05, (Student's t-test).

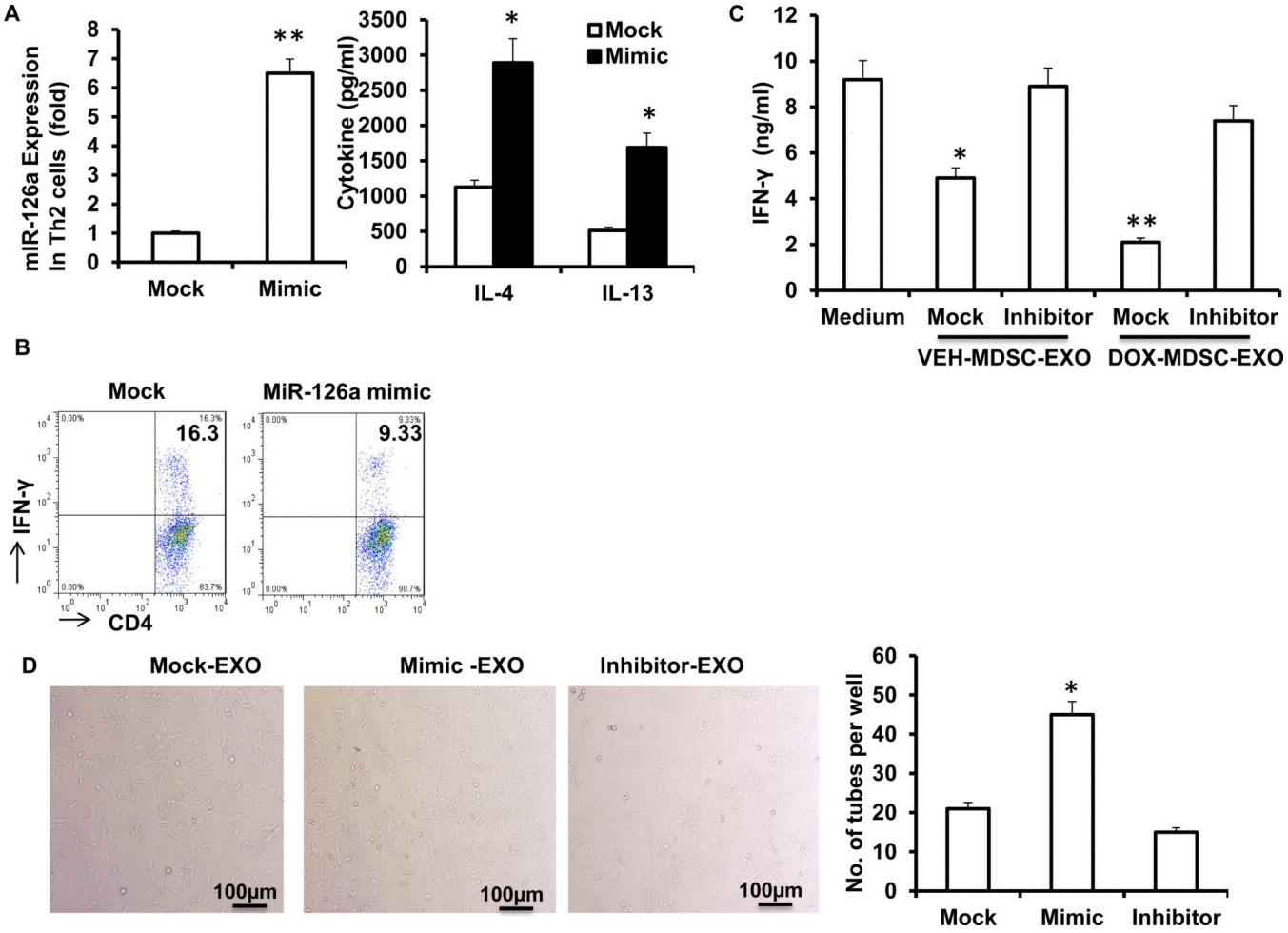

Figure 4. Exosomes of DOX-MDSCs regulate proangiogenic effects and T cell activity via miR-126a

A–B) $CD4^+$ T cells were transfected with miR-126a mimic in the presence of 5μg/ml anti-CD3, 5μg/ml anti-CD28 and 10μg/ml anti-IFN-γ (A) or 10μg/ml anti-IL-4 (B). The expression of miR-126a and the level of cytokines in Th2 cells were examined by RT-PCR (A, left) or ELISA (A, right) or the expression of IFN- γ in Th1 cells were examined by FACS (B). **C**) $CD4^+$ T cells were co-cultured with exosomes isolated from mock or miR-126a inhibitor-transfected VEH-MDSCs or DOX-MDSCs in the presence of 5μg/ml anti-CD3, 5μg/ml anti-CD28 and 10μg/ml anti-IL-4 for 4 days. The level of IFN-γ in the supernatant of co-cultured cells was determined by ELISA. Data are mean ± SEM. *P<0.05, **P<0.01 (Student's t-test). **D**) In vitro tube-formation assay of MDSC exosomal miR-126a. ECs were co-cultured with exosomes isolated from mock, miR-126a inhibitor or mimic-transfected MDSCs. Representative micrographs are shown (left). The number of tube-like structures was counted per well of 48-well plates (right). Data are mean ± SEM of 3 independent experiments. $^*p < 0.05$, (Student's t-test).

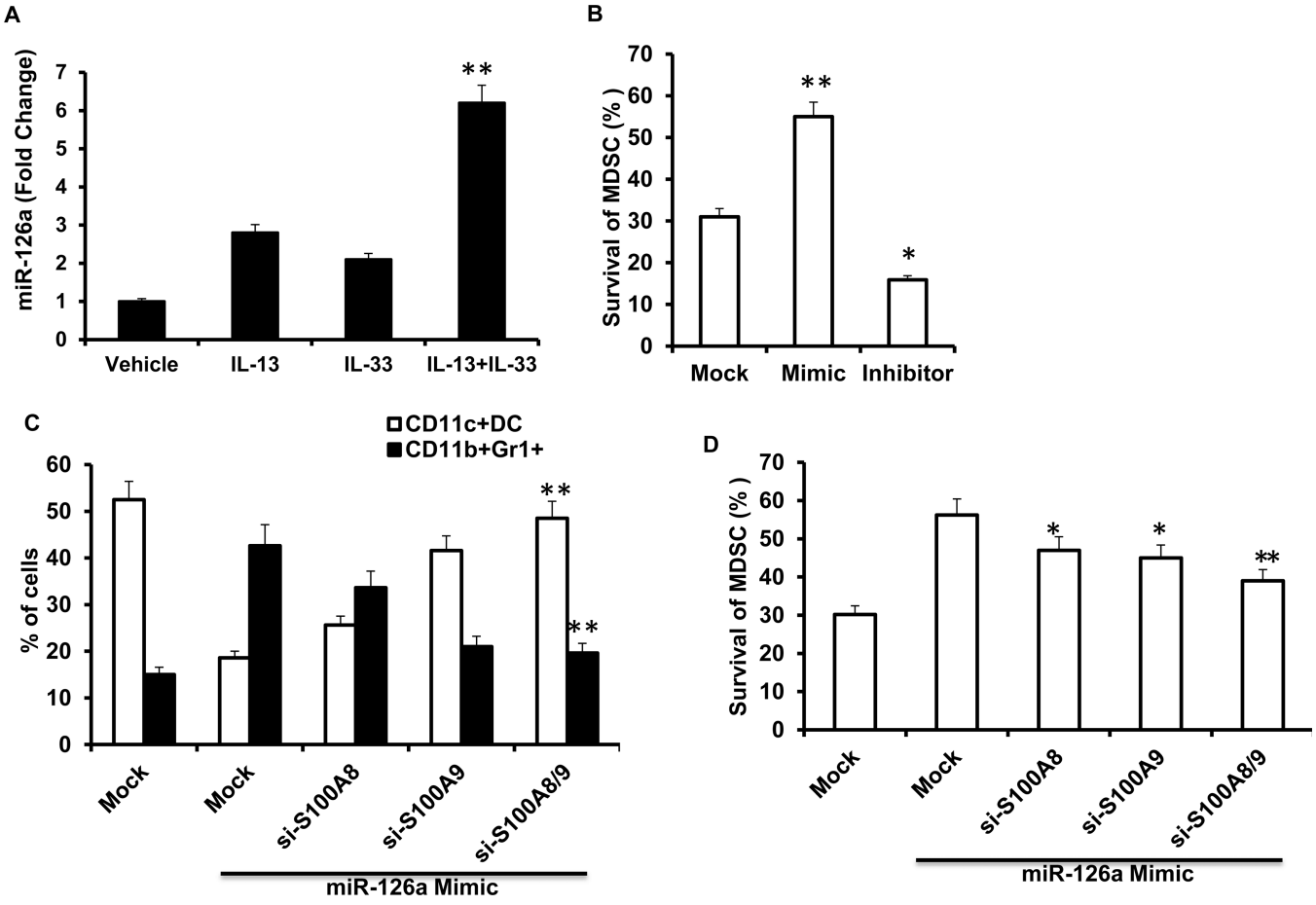

Figure 5. miR-126a promotes the accumulation of MDSCs under chemotherapy via S100A8/9

A) Immature myeloid cells in the lung from naïve mice were stimulated with IL-13, IL-33 or both. The expression of miR-126a was quantified by RT-PCR. **B**) Survival of naïve MDSCs treated by 20nM doxorubicin in the presence of exosomes derived from MDSCs transfected with 100 nM miR-126a inhibitor, 100 nM mimic or mock. Viability and cell number were determined by propidium iodide exclusion. **C**) Phenotypes of cells generated from bone marrow progenitor cells by 5-d cultures with GM-CSF and IL-4. Bone marrow progenitor cells were transfected with mock or miR-126a mimic without/with siRNA for S100A8, S100A9, or a combination of S100A8 and 9 (S100A8/9). **D**) Survival of cells generated from C treated by 20nM doxorubicin. Data represent means ± SEM. $^{*}p < 0.05$,$^{**}p < 0.01$, (Student's t-test).

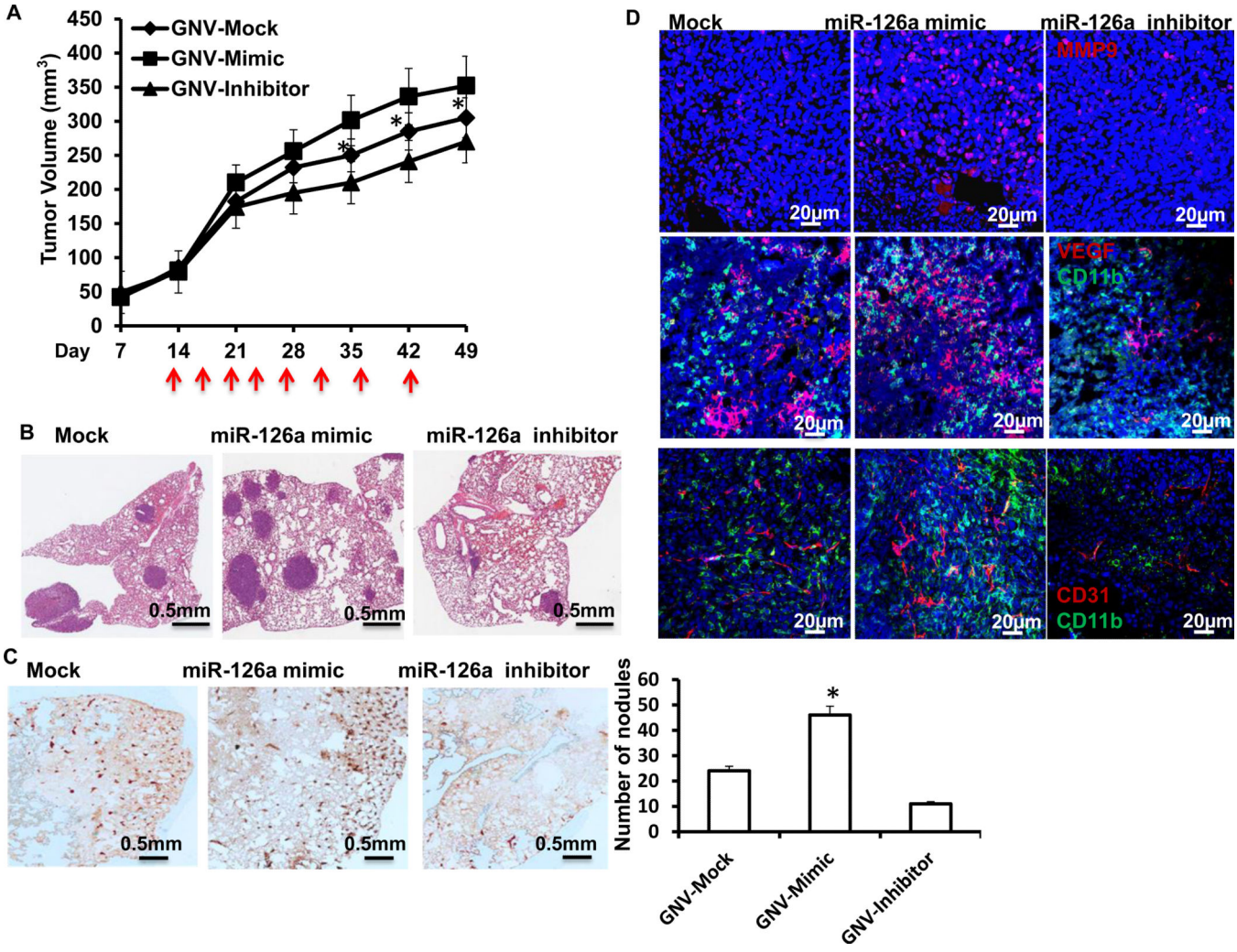

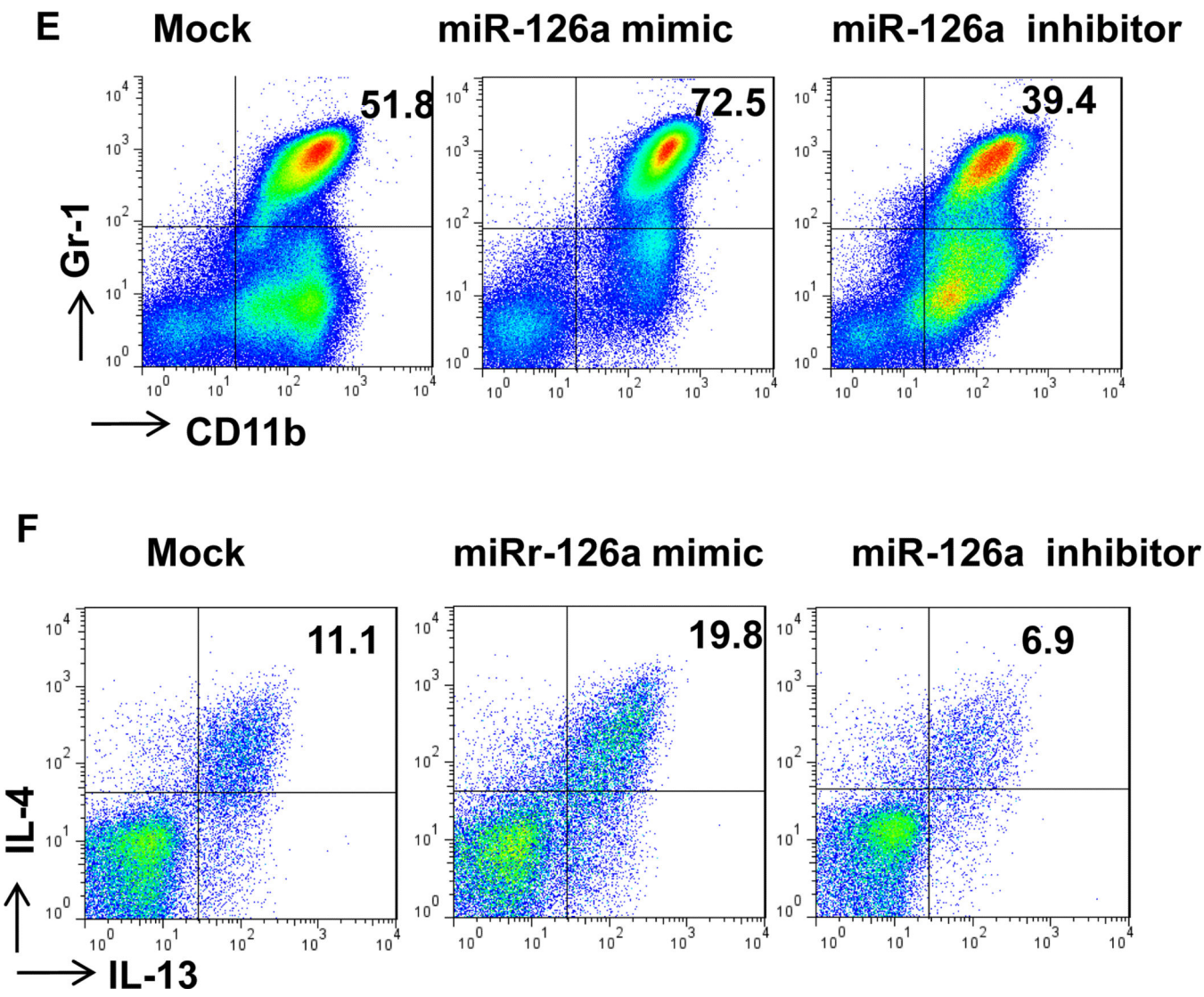

Figure 6. Concurrent deliveries of miR-126a inhibitor and Doxorubicin suppress lung metastasis of breast cancer via regulating the MDSC and Th2 cell responses

A) Tumor growth in 4T1 tumor-bearing mice. Ten days after tumor initiation, mice were treated by Doxorubicin and dosed with 1.5 mg/kg of mock, miR-126a inhibitor or miR-126a mimic for eight doses. Arrowheads indicate time points of nanoparticle and Doxorubicin administration. Data are mean ± SEM, (n=7). **P* < 0.05. **B**) Representative histology staining of lung from 4T1 tumor-bearing mice treated by Doxorubicin combination with mock, miR-126a inhibitor, or miR-126a mimic. **C**) The lungs were stained for vimentin (right). Total number of nodules/lung shown (left). Data represent means ± SEM. $^{*}p < 0.05$, (Student's t-test). **D**) Immunohistochemical detection of CD31, MMP9, VEGF (red) and CD11b (green) in lung from treated 4T1 tumor bearing mice. **E**) Representative FACS analysis of MDSC in lung. **F**) Representative FACS analysis of the expression IL-4 and IL-13 in lung $CD4^{+}$ T cells.